Bicarbonate Is a *Native* Cofactor for Assembly of the Manganese Cluster of the Photosynthetic Water Oxidizing Complex. Kinetics of Reconstitution of O_2 Evolution by Photoactivation[†,‡]

S. V. Baranov,[§,||] A. M. Tyryshkin,[§] D. Katz,[§] G. C. Dismukes,*[,§] G. M. Ananyev,[⊥] and V. V. Klimov[#]

Department of Chemistry, Hoyt Laboratory, Princeton University, Princeton, New Jersey 08544, Institute of Marine and Coastal Sciences, Rutgers University, 71 Dudley Road, New Brunswick, New Jersey 08901, and Institute of Basic Biological Problems, Russian Academy of Sciences, Pushchino, Moscow Region, 142290 Russia

Received May 22, 2003; Revised Manuscript Received December 31, 2003

ABSTRACT: Assembly of the inorganic core ($Mn_4O_xCa_1Cl_y$) of the water oxidizing enzyme of oxygenic photosynthesis generates O_2 evolution capacity via the photodriven binding and photooxidation of the free inorganic cofactors within the cofactor-depleted enzyme (apo-WOC−PSII) by a process called photoactivation. Using in vitro photoactivation of spinach PSII membranes, we identify a new lower affinity site for bicarbonate interaction in the WOC. Bicarbonate addition causes a 300% stimulation of the rate and a 50% increase in yield of photoassembled PSII centers when using Mn^{2+} and Ca^{2+} concentrations that are 10−50-fold larger range than previously examined. Maintenance of a fixed Mn^{2+}/Ca^{2+} ratio (1:500) produces the fastest rates and highest yields of photoactivation, which has implications for intracellular cofactor homeostasis. A two-step (biexponential) model is shown to accurately fit the assembly kinetics over a 200-fold range of Mn^{2+} concentrations. The first step, the binding and photooxidation of Mn^{2+} to Mn^{3+}, is specifically stimulated via formation of a ternary complex between Mn^{2+}, bicarbonate, and apo-WOC−PSII, having a proposed stoichiometry of [$Mn^{2+}(HCO_3^-)$]. This low-affinity bicarbonate complex is thermodynamically easier to oxidize than the aqua precursor, [Mn^{2+}-(OH_2)]. The photooxidized intermediate, [$Mn^{3+}(HCO_3^-)$], is longer lived and increases the photoactivation yield by suppressing irreversible photodamage to the cofactor-free apo-WOC−PSII (photoinhibition). Bicarbonate does not affect the second (rate-limiting) dark step of photoactivation, attributed to a protein conformational change. Together with the previously characterized high-affinity site, these results reveal that bicarbonate is a multifunctional "native" cofactor important for photoactivation and photoprotection of the WOC−PSII complex.

The participation of dissolved carbon dioxide, often as the bicarbonate or carbonate ions, in light-driven electron transport processes in oxygenic photosynthesis has been a rich field of study for more than 30 years, in part because these species could serve in a feedback mechanism for controlling the delivery of reducing equivalents to the (dark) carbon fixation reaction (reviewed in ref *1* and references cited therein). There are several sites for bicarbonate/CO_2 action in photosynthesis. Here we focus on those found in or around PSII. On the basis of spectroscopic data (*2*, *3*) it was concluded that bicarbonate binds to the non-heme Fe(II) site of photosystem II (PSII)[1] as a ligand to the non-heme iron (*4*, *5*) where it supports rapid electron transfer between the quinone cofactors Q_A and Q_B, possibly through facilitating proton transfer steps (*6*). Evidence for a second site in PSII where bicarbonate acts has also been revealed (*7*). The idea of the possible involvement of bicarbonate in the water oxidation/O_2 evolution reaction was first hypothesized by Warburg (*8*) and later by Stemler and Govindjee (*9*). Mass spectrometric data (*10*) and biochemical data (*11*) that support the hypothesis were given and later refuted by other mass spectrometric data (*12*). More recent biochemical evidence was interpreted in favor of a carbonic anhydrase activity intrinsic to PSII as a possible origin for the bicarbonate effect on PSII (*13*, *14*).

[†] This work was supported by grants from the National Institutes of Health (GM 39932) and the Human Frontiers Science Program (RGP0029) and by an international cooperation grant from the NIH−Fogarty program (RO3 TWO5553-01). Instrumentation fabrication was supported by a grant from the National Science Foundation (DBI-0138012).

[‡] In memory of George Cheniae.

* Address correspondence to this author. Phone: 609-258-3949. Fax: 609-258-1980. E-mail: dismukes@princeton.edu.

[§] Princeton University.

[||] On leave from the Institute of Basic Biological Problems, Russian Academy of Sciences, Pushchino, Moscow Region, 142290 Russia.

[⊥] Rutgers University.

[#] Russian Academy of Sciences.

[1] Abbreviations: Chl, chlorophyll; DCBQ, 2,5-dichloro-*p*-benzoquinone; EP-depleted PSII, PSII membranes depleted of the extrinsic proteins; EPR, electronic paramagnetic resonance; LED, light-emitting diode; MES, 2-(*N*-morpholino)ethanesulfonic acid; PSII, photosystem II; WOC, water-oxidizing complex; Y_{SS}, steady-state yield of photoactivation process.

10.1021/bi034858n CCC: $27.50
Published on Web 01/28/2004

The evidence for bicarbonate involvement on the donor side of PSII has been recently summarized (*15*). Bicarbonate was shown to stimulate the rate of donation of electrons from free Mn^{2+} ions to the photogenerated tyrosine radical $Y_Z^{\bullet}$ in manganese-depleted PSII. Bicarbonate addition to Mn-depleted PSII facilitates the photoconversion of added Mn^{2+} into a form that is not detectable by conventional (perpendicular mode) EPR at room temperature and is presumed to be in the form of Mn^{3+} (*16*). EPR data have since confirmed that Mn^{3+} forms as the product of Mn^{2+} photooxidation by apo-WOC−PSII (*17*). Electrochemical data have provided evidence to support the involvement of Mn−bicarbonate complexes as the likely electron donors (*18*). These studies have helped to clarify the earlier contradictory claims but have not identified where and how bicarbonate acts to stimulate water splitting by PSII.

The inorganic cofactors required for O_2 evolution activity by the native PSII−WOC have been previously identified by examining the recovery of O_2 evolution activity to the cofactor-depleted WOC−PSII (apo-WOC−PSII). This process, termed photoactivation, is a multistep process that requires both light and dark steps in the presence of the free inorganic ions (Mn^{2+}, Ca^{2+}, Cl^-), an exogenous electron acceptor (ferricyanide, DCIP), and apo-WOC−PSII (*19*). Although performed in vitro, this process is believed to model the in vivo pathway of assembly during biogenesis and repair (*20*, *21*). In the last several years it has become possible to kinetically resolve the first few steps during photoactivation by monitoring the rate of reconstitution of O_2 evolution using ultrasensitive amperometric detection of O_2 with improved time resolution (*22*, *23*). This has led to the elaboration of the two-step kinetic model that was proposed on the basis of O_2 yield measurements (*24*−*27*).

Using this method we previously found a small (10−20%) but consistent effect of bicarbonate on the kinetics and yield of photoactivation when using stoichiometric amounts of Mn^{2+} (2−4 Mn^{2+}/PSII) at the 1−4 μM concentration range (*28*). This work demonstrated the existence of a high-affinity binding site (K_D < 10 μM) for bicarbonate within apo-WOC−PSII which accelerates formation of the first Mn^{3+} assembly intermediate from Mn^{2+}. However, it has remained unclear how bicarbonate may differ from other weak bases or hydroxide donors and what its effect may be at much higher (physiological) concentrations [dissolved inorganic carbon in water arising from atmospheric CO_2 is less than 15 μM versus 2 mM in seawater, while intracellular levels of 0.5 mM are found in some freshwater cyanobacteria (*29*)]. For example, alkaline pH also accelerates the initial rate of photoactivation but, in contrast to bicarbonate, reduces the yield or activity of fully reconstituted centers (*30*). Herein we examine the effect of bicarbonate on photoactivation kinetics using concentrations of Mn^{2+} up to 250 molar excess and Ca^{2+} up to 10^5 molar excess over the apo-WOC−PSII concentration. These concentrations are 50-fold and 10-fold higher, respectively, than we previously examined and set the stage for future spectroscopic measurements under identical conditions. At these higher Mn^{2+} and Ca^{2+} concentrations, bicarbonate produces a much greater rate acceleration and stimulates the yield of the assembly process more so than at stoichiometric Mn^{2+}/PSII ratios. These larger effects correspond to a new (low affinity, $K_D = 0.2-2$ mM) site for bicarbonate interaction with Mn^{2+} bound to PSII that is distinct from the high-affinity site reported earlier (K_D < 10 μM). Thus, the present and earlier data indicate two sites for bicarbonate functioning during assembly of the inorganic core in the WOC of PSII. The data presented herein show a close association between the low-affinity bicarbonate site and the high-affinity Mn^{2+} site on apo-WOC−PSII. We discuss possible chemical models for this ternary complex and evolutionary implications.

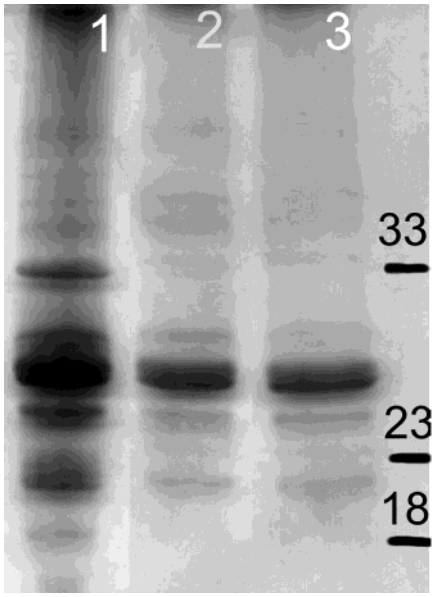

FIGURE 1: Extrinsic protein composition of the PSII membrane preparations used in this study resolved by SDS−PAGE containing 13.5% acrylamide: lane 1, PSII membranes; lane 2, the EP-depleted PSII membranes; lane 3, apo-WOC−PSII membranes. The numbers to the right represent molecular masses (in kDa) deduced from molecular weight markers (Sigma).

MATERIALS AND METHODS

PSII-enriched membrane fragments were prepared from market spinach by the method of Berthold et al. (*31*) with minor modifications (*32*). Under saturating continuous illumination, the oxygen evolution rate of the PSII membranes was 400−450 μmol of O_2/(mg of Chl·h) in the presence of 1 mM $K_3Fe(CN)_6$ and 0.25 mM 2,5-dichloro-*p*-benzoquinone (DCBQ) as electron acceptors. Membranes at 3−5 mg of Chl/mL were frozen in 0.4 M sucrose−MES/NaOH buffer (pH 6.0) and stored in liquid N_2. SDS−PAGE was performed using a 13.5% gel with PSII samples containing 10−15 μg of Chl/mL in accordance with the literature (*33*).

PSII membranes depleted of all three extrinsic proteins (molecular mass 17, 24, and 33 kDa) but retaining all four manganese ions were obtained by washing in 1 M $CaCl_2$ using the method of Ono et al. (*34*). In the presence of 20 mM $CaCl_2$, these extrinsic protein-depleted PSII (EP-depleted PSII) membranes exhibit a 60% oxygen evolution rate versus the untreated PSII membranes at pH 6.0, in agreement with these authors (data not shown). SDS−PAGE of EP-depleted PSII membranes confirms complete removal of all three extrinsic proteins (Figure 1) and thus reveals that they have the same protein composition as the apo-WOC−PSII particles used in the photoactivation experiment. Therefore, we used the O_2 evolution rate of EP-depleted samples as a measure of the maximal rate which may be reached if 100% of apo-WOC−PSII membranes were reconstituted. Accord-

ingly, the vertical scale in the O_2 measurements shown in this paper is normalized to the activity of the EP-depleted PSII particles measured under identical cofactor concentrations, pH, and illumination conditions. The vertical scales reflect the absolute percentage yield of reactivated PSII membranes in photoactivation experiments.

To prepare apo-WOC−PSII samples depleted of Mn^{2+}, Ca^{2+}, and the three extrinsic proteins, we used a brief incubation in mild alkaline buffer as previously described (*35*) with some modifications (*36*). This method is based upon observations that alkaline treatment for short periods inactivates O_2 evolution reversibly (*19*, *37*, *38*). Small volumes (∼1 mL) of PSII membranes at a concentration of 0.25 mg of Chl/mL were incubated in 20 mM CHES/NaOH buffer (pH 9.4) in the presence of 200 mM $MgCl_2$ for 40−90 s at room temperature followed by dilution with 50 mM MES/NaOH buffer (pH 6.0) to stop the reaction. The membranes were washed with 0.3 M sucrose−MES/NaOH buffer (50 mM, pH 6.0) in the presence of 1 mM EDTA and twice in the EDTA-free buffer. The resulting apo-WOC−PSII membranes were devoid of the three extrinsic proteins as determined by SDS−PAGE (Figure 1) and exhibited no residual O_2 evolution activity (i.e., below the detection limit of the photoactivation cell, 0.5% peak or 0.05% peak integral). The residual Mn content in these apo-WOC−PSII membranes was estimated to be less than 0.3 Mn per PSII, using EPR to detect free Mn^{2+} following acid digestion in 100 mM HNO_3 and assuming 250 Chl/PSII. These apo-WOC−PSII particles were capable of reconstituting the water-splitting system of PSII and to evolve oxygen at very high rates equal to 60−70% of the rate observed with the EP-depleted PSII, or about 40% of the O_2 rate of the untreated PSII complexes.

Photoactivation of apo-WOC−PSII membranes was performed as previously described (*30*) in assay medium containing 300 mM sucrose, 35 mM NaCl, and 50 mM MES/NaOH buffer (pH 6.0) and in the presence of 1.8 mM $K_3Fe(CN)_6$ as the terminal electron acceptor. The samples (1 μM apo-WOC−PSII and an indicated amount of $MnCl_2$, $CaCl_2$, and $NaHCO_3$) were mixed, loaded into the photoactivation cell, and incubated for 11 min in the dark prior to the start of the illumination. Light pulses from an LED (wavelength maximum 670 nm and peak intensity 80 mW/cm^2) were used with constant duration (t_{light} = 30 ms) and fixed dark time between flashes (t_{dark} = 3 s). The same light flashes were used both to advance the light-dependent photoassembly reaction and to measure the O_2 evolution rate of the assembled WOC−PSII. Amperometric detection of O_2 was performed in a Clark-type microcell of 5 μL volume covered with a thin (1−5 μm) silicone-type membrane having a rise time of 0.1 s for O_2 detection. Differential amplification of the signal in the bandwidth 0.3−10 Hz was used to further reduce the noise level (S/N ∼ 5 at 50 fmol of O_2). Additionally, a computer-based digital acquisition system allowed 10 point averaging (at 5 kHz sampling rate) to further improve the S/N. The resulting O_2 signal was postprocessed by integration to give the total O_2 evolved per each flash. The final S/N ratio of the integrated peak permits detection of about 0.05% of the O_2 signal produced by the holoenzyme. The time course of the O_2 signal recovery was normalized to the O_2 evolution activity per flash of the EP-depleted PSII (as described above) to give a percentage yield of the reactivated WOC−PSII. Finally, the resulting integrated kinetic curves were fitted by a linear multiexponential model using a commercial software package Origin 7.0 (OriginLab).

RESULTS

Kinetic Model of Photoactivation. The minimal kinetic model to describe the photoactivation process consists of two steps (*23*, *24*, *27*, *39*):

$$IM_0 \underset{k_{-1}}{\overset{k_1}{\rightleftharpoons}} IM_1 \xrightarrow{k_2} IM_2 \xrightarrow{\text{fast}} WOC{-}PSII \qquad (1)$$

where IM_0 is a dark precursor state, IM_1 and IM_2 are assembly intermediates, and WOC−PSII is the reconstituted (functional) oxygen evolving complex. At low Mn^{2+} concentrations typically used in our works (1−16 μM), the dark precursor IM_0 is mostly free of Mn^{2+}, e.g., apo-WOC−PSII (*23*). At greater Mn^{2+} concentrations used by others (0.1−1 mM), IM_0 has Mn^{2+} bound to the high-affinity site in PSII (*24*, *27*). Depending on the initial dark precursor state, the first reversible step ($k_{1/-1}$) involves binding and/or light-induced photooxidation of Mn^{2+} to Mn^{3+} to form the first assembly intermediate, IM_1. Confirmation of this step to include the first assembly intermediate IM_1 was possible following improved kinetic resolution (*23*).

The second step (k_2) is kinetically rate-limiting. It was shown to involve both dark and light steps that produce a long-lived intermediate IM_2 containing two Mn^{3+} (*23*, *24*, *27*, *40*). The systematic study of the dependence of k_2 on Mn^{2+} and Ca^{2+} concentrations and on various light−dark flash regimes led us to conclude that a dark step, forming intermediate IM_1*, precedes the light-dependent step of binding and photooxidation of the second Mn^{2+} (*22*, *23*):

$$IM_0 \underset{k_{-1}}{\overset{k_1}{\rightleftharpoons}} IM_1 \xrightarrow{k_2} IM_1^* \xrightarrow{\text{fast}} IM_2 \rightarrow WOC{-}PSII \qquad (2)$$

The dark step is actually rate-limiting, and its slowness may be associated with a protein conformational change that prepares the binding site for the uptake of the second Mn^{2+} (*27*, *39*). An alternative model for the rate-limiting step has been also postulated. This step was suggested to proceed via an unstable intermediate that contains one Mn^{3+} and one Mn^{2+} (*24*, *26*, *27*, *40*). Since the decay time of this unstable intermediate is fast, it may form and decay many times before advancing with a low efficiency to the next stable intermediate IM_2. Thus, the overall slowness of the rate-limiting step k_2 was explained by the low quantum efficiency of the reaction.[2] The difference in the two models probably arises owing to the 10−100 times greater Mn^{2+} concentrations used in these works. The assembly of the $(Mn)_4$ cluster is completed by binding and oxidation of two more Mn^{2+} ions, which is fast and therefore kinetically unresolved.

Each kinetic step in eq 1 may involve a number of chemical steps and require one or more cofactors (e.g., such as Mn^{2+}, Ca^{2+}, Cl^-), a loss of proton, and either light or darkness. For simplicity, each photoactivation step is described by the pseudo-first-order rate constants (k_i) which

[2] Note that the rate-limiting step k_2 in eq 1 is not equivalent to the rate-limiting (or yield-determining) step k_D in the model proposed by Tamura and Cheniae (*24*).

explicitly include the dependence on the cofactor concentrations, media pH, and light/dark intensity regime. The cofactor and light requirements for the first two kinetically resolved steps ($k_{\pm1}$ and k_2) have been previously examined (see refs *23* and *39* and references cited therein). Under the condition that all steps after IM_2 are much faster, and assuming that the concentrations of the added Mn^{2+} and Ca^{2+} cofactors do not change significantly during the course of the photoactivation process (and thus k_i are constant), the model of eq 1 has the analytical solution:

$$Y(t) = Y_{SS} + A_1 e^{-\lambda_1 t} - A_2 e^{-\lambda_2 t} \quad (3)$$

where $A_1/\lambda_2 = A_2/\lambda_1 = Y_{SS}/(\lambda_1 - \lambda_2)$, $Y(t)$ is the yield of the assembled WOC−PSII at time t, and Y_{SS} is the steady-state yield extrapolated to infinite time. The rate constants $\lambda_{1,2}$ are complex functions of the rate constants $k_{\pm1}$, k_2:

$$\lambda_{1,2} = \frac{(k_1 + k_{-1} + k_2) \pm \sqrt{(k_1 + k_{-1} + k_2)^2 - 4k_1k_2}}{2} \quad (4)$$

At commonly encountered conditions of the photoactivation experiments, $k_1 \gg k_2$, these expressions can be simplified to $\lambda_1 = (k_1 + k_{-1})$ and $\lambda_2 = k_2k_1/(k_1 + k_{-1})$. $Y(t)$ is directly proportional to the O_2 flash yield, $[O_2(t)] = Y(t)\Phi$, where Φ is the quantum yield of O_2 per flash per unit concentration of reconstituted WOC−PSII centers. As indicated in Materials and Methods, for the purpose of normalization Φ is assumed to be equivalent to the same value obtained using the EP-depleted PSII complexes, measured under identical conditions. Thus, the yield of reactivated PSII centers in eq 3 is obtained from $[O_2(t)]/\Phi$.

Typical experimental kinetics of reconstitution of O_2 evolution by photoactivation of apo-WOC−PSII are shown in Figure 2, using 400 light/dark pulse cycles. Panel A illustrates the kinetics in the presence of 250 molar excess of $MnCl_2$ (250 μM) and 100 mM $CaCl_2$ (curve 1) and in the absence of either Mn^{2+} or Ca^{2+} (curve 2). The vertical scale is normalized to 100% of the photoactivation yield, using the EP-depleted PSII particles as described in Materials and Methods. Thus, about 70% of apo-WOC−PSII was reconstituted with a functional WOC in experiment 1 in Figure 2, while no detectable O_2 activity is seen in experiment 2 in the absence of added Mn^{2+} or Ca^{2+}. Two phases (lag phase and the rate-limiting λ_2 phase) are clearly resolved in the photoactivation kinetics. Note that in our previous works we mainly used graphical methods to obtain the parameters k_2 and the lag time (t_{lag}) directly from the plots of the experimental kinetics using the method of initial rates (*23*). Herein, we use a least-squares numerical method to fit the entire time course of photoactivation kinetics to eq 3. Both methods provide essentially the same results; however, uncertainty of the graphical method (arising from necessity to guess Y_{SS} to achieve the best linearization of the kinetics in the log graph plot) is avoided in the numerical fitting. For the case $\lambda_1 \gg \lambda_2$, which is typical for many of our experiments, the relationship between these parameters is simply given by $\lambda_1 \sim 1/t_{lag}$ and $\lambda_2 \sim k_2$. The lag period t_{lag} and Y_{SS} derived from the numerical fit (see below) are also indicated in Figure 2. Here and in all other fittings, Y_{SS} was obtained by extrapolation of a biexponential fit to infinite time, using experimental kinetic data that are at least 80% complete. Panel B expands the initial portion of the kinetics from panel A. Small (negative) flash artifacts are clearly seen in curves 1and 2 which can be nearly fully eliminated by subtracting curve 1 − curve 2.

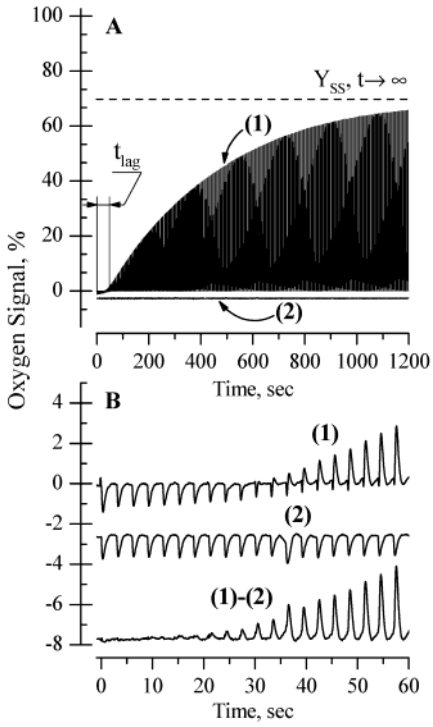

FIGURE 2: (A) Kinetics of restoration of flash-induced O_2 evolution (photoactivation) in cofactor-depleted apo-WOC−PSII in the presence of 250 μM $MnCl_2$, 100 mM $CaCl_2$, and 1.8 mM $K_3Fe(CN)_6$ (curve 1) and in the absence of the cofactors (curve 2). 400 flashes (~20 min) are shown. The lag time (t_{lag}) is computed from a biexponential fitting of the integrated kinetics using eq 2. The horizontal dashed line indicates the maximum yield of O_2 at the end of photoactivation (Y_{SS}) estimated by numerical fitting. The vertical scale (100%) is normalized to absolute yield of reactivated PSII centers as described in the text. (B) Expanded first minute of the kinetics from panel A in the presence (1) and in the absence (2) of Mn^{2+}/Ca^{2+} cofactors. Subtraction of curve 1 − curve 2 eliminates the flash artifact.

This artifact-corrected curve was integrated to determine the O_2 evolved per flash and then was numerically fitted to eq 3. An example of such a fit is shown in Figure 3 and confirms that the biexponential model given by eq 3 fits the data to within better than 1% residual, which is equal to the random error of the data. Taking into account our earlier measurements at low cofactor concentrations, we find that the biexponential model fits the kinetics over the range 4−250 Mn^{2+}/PSII (8−250 μM Mn^{2+}) and 8−300 mM Ca^{2+}. This represents a 10−50-fold wider concentration range than examined by this method previously (*23*).

High Mn^{2+} and Ca^{2+} Concentrations. Previous studies have already established that maintaining an optimal ratio of Mn^{2+} and Ca^{2+} concentrations is essential for effective reactivation of WOC−PSII (*25*, *27*, *41*). Confirming this earlier work, we found that 0.1−0.5M Ca^{2+} is required to produce the maximum yield at 100−250 μM Mn^{2+}. This is a 12−50-fold increase above the 8 mM Ca^{2+} found optimal when using stoichiometric levels of Mn^{2+} (4−16 μM) (*23*). Remarkably, at 250 μM Mn^{2+} and 100 mM Ca^{2+} the yield of assembled PSII, $Y_{SS} = 50-70\%$, is significantly improved compared to only 20−30% at 10 μM Mn^{2+} and 8 mM Ca^{2+}

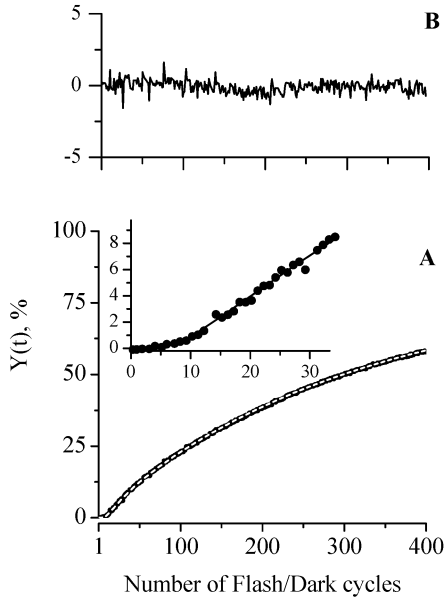

FIGURE 3: Integrated O_2 flash yield during photoactivation as performed in Figure 1. (A) Experimental and simulated (superposed solid line) photoactivation kinetics and (B) their residual plot. The simulation uses the biexponential model of eq 3. The insert in panel A represents the first 35 flashes (solid circles). The vertical scale is normalized to 100% of photoactivation yield using the EP-depleted particles. Conditions are the same as in Figure 2.

Table 1: Representative Kinetic Parameters for Photoactivation at Low and High Concentrations of the Mn^{2+} and Ca^{2+} Cofactors[a]

cofactors[b]	Y_{SS}[c] (%)	λ_1, s^{-1}	λ_2, s^{-1}
10 μM Mn^{2+} and 8 mM Ca^{2+} [d]	20−30	0.03	0.0015
250 μM Mn^{2+} and 100 mM Ca^{2+}	50−70	0.06	0.0007

[a] In both cases, at the given Ca^{2+} concentration the Mn^{2+} concentration was optimized to produce the highest yield of photoactivation with no added bicarbonate. [b] See Materials and Methods for pH, buffer, and electron acceptor concentrations. [c] The highest yield found so far (75%) occurs at 250 μM $MnCl_2$, 100 mM $CaCl_2$, and 125 μM bicarbonate, pH 6.0. [d] The rate constants λ_1 and λ_2 shown at low Mn^{2+}/Ca^{2+} concentrations differ slightly from what we reported earlier (see, for example, ref *23*) because of different illumination conditions (light pulses of 30 ms in this study versus 40 ms in ref *23*) and different pH (6.0 vs 6.2).

(Table 1). In earlier works we reported 100% photoactivation yield based on a less accurate normalization standard, involving comparison to the O_2 evolution rate of intact PSII membrane using continuous light illumination (*22*). The use of even higher manganese concentrations does not increase the yield at any Ca^{2+} concentration. In addition, above 250 Mn^{2+} per PSII (250 μM) we observe that a third exponential component appears in the photoactivation kinetics (data not shown), and thus the model given by eq 1 is not strictly valid above this concentration range. Therefore, we restricted our study to concentrations no higher than 250 μM Mn^{2+}.

Over the concentration range from 10 to 250 μM Mn^{2+} the kinetic parameters (λ_1 and λ_2) do not change by more than a factor of 2, provided that the Ca^{2+} concentration is adjusted to optimize the yield (Table 1). This observation is consistent with previous data suggesting a competition or screening between Mn^{2+} and Ca^{2+} taken up during the photoactivation process (*20*, *23*, *25*, *27*).

Effect of Bicarbonate. Figure 4 plots representative integrated photoactivation kinetics, $Y(t)$, obtained from data

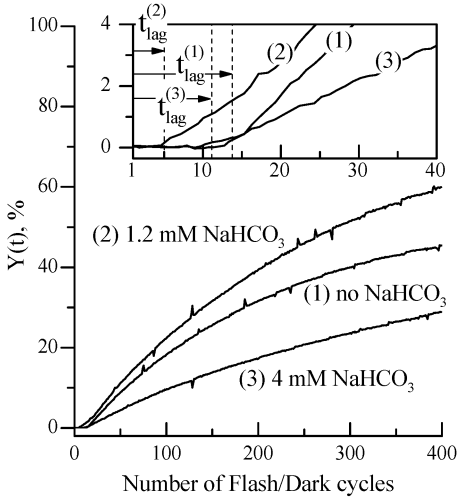

FIGURE 4: Photoactivation kinetics of apo-WOC−PSII membranes in the presence of (1) 0 mM, (2) 1.2 mM, and (3) 4 mM added bicarbonate. Assay conditions are pH = 6.0, 1 μM apo-WOC−PSII, 100 μM $MnCl_2$ (100 Mn^{2+}/PSII), 100 mM $CaCl_2$, and 1.8 mM $K_3Fe(CN)_6$. The insert expands the first 40 flashes. The vertical dashed lines represent the lag time $t_{lag}^{(i)}$ for each experiment as derived from fitting the entire kinetics to eq 3.

like those in Figure 2, measured in the presence of 0, 1.2, and 4 mM added sodium bicarbonate at fixed pH 6.0 and with 100 μM Mn^{2+} and 100 mM Ca^{2+}. The kinetics have noticeably different slopes and lag times (t_{lag} is shown more clearly in the insert in Figure 4). The kinetic parameters (Y_{SS}, λ_1, λ_2) were derived from the numerical fits of the data to the biexponential model of eq 3, and these parameters are summarized in Figure 5 for three different Mn^{2+} concentrations at fixed 100 mM Ca^{2+} and as a function of the bicarbonate concentration up to 4 mM. Higher bicarbonate concentration led to a shift of the pH, and therefore data above 4 mM are not included.

Figure 5A shows that bicarbonate stimulates the photoactivation yield Y_{SS} by 70% at 16 μM $MnCl_2$, by 50% at 100 μM $MnCl_2$, and by 24% at 250 μM $MnCl_2$, as compared to the samples without added bicarbonate (there is about 6 μM bicarbonate due to dissolved atmospheric CO_2 at pH 6.0). At 250 μM $MnCl_2$ and 125 μM bicarbonate, Y_{SS} reaches a maximum level of 75%, which is the highest yield observed in any photoactivation experiment we have reported. Noteworthy, the data in Figure 5A show that the amount of bicarbonate needed to maximize the yield is reduced in proportion to the amount of Mn^{2+} in the medium. Y_{SS} peaks at bicarbonate ≥4 mM (16 Mn^{2+}/PSII), 1 mM (100 Mn^{2+}/PSII), and 0.2 mM (250 Mn^{2+}/PSII). Independently, we observed that added bicarbonate does not affect the flash-induced O_2 yield of the EP-depleted PSII membranes at bicarbonate concentrations up to 4 mM (data not shown). Therefore, the 100% level in Figure 5A is identical at all bicarbonate concentrations between 6 μM (the atmospheric content) and 4 mM.

Comparison of Figures 5A and 4B reveals that the stimulation of Y_{SS} is closely correlated to acceleration of λ_1 (the rate constant for formation of the first intermediate), as judged by the parallel trends of their Mn^{2+} and bicarbonate concentration dependences. In the case of 16 and 100 μM Mn^{2+}, addition of 4 mM bicarbonate results in 4- and 3-fold acceleration of λ_1, respectively, while at 250 μM Mn^{2+} the

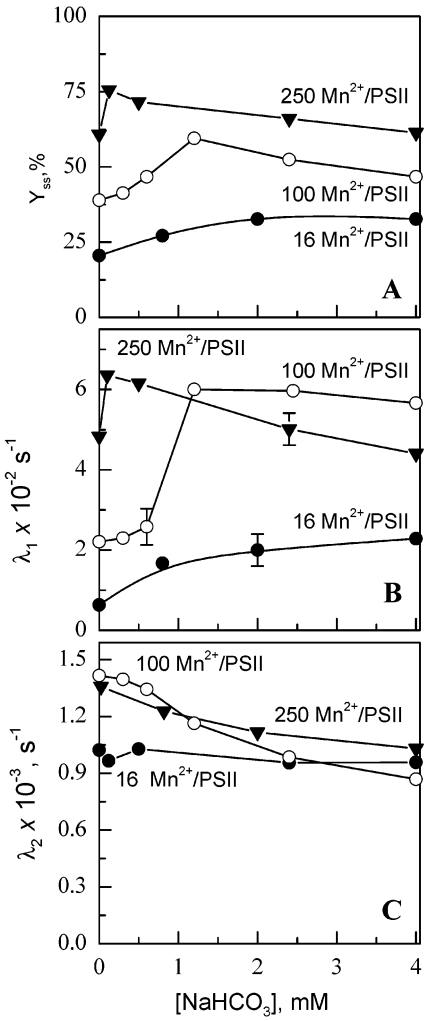

FIGURE 5: Bicarbonate concentration dependence of (A) the photoactivation yield, Y_{SS}, (B) the pseudo-first-order rate constant for formation of the first intermediate, λ_1, and (C) the pseudo-first-order rate constant for the rate-limiting step, λ_2. Assay conditions: pH = 6.0, 1 μM apo-WOC−PSII, 100 mM $CaCl_2$, and indicated concentrations of $MnCl_2$.

acceleration is about 1.3-fold. The bicarbonate concentration required to produce this maximal acceleration decreases in direct proportion to the Mn^{2+} concentration in the medium.

Figure 5C demonstrates that the rate constant λ_2 (the rate-limiting step) is virtually unaffected by bicarbonate. A small decrease of λ_2 is observed at the higher bicarbonate concentrations, with the maximal effect of 30% seen at 100 μM Mn^{2+} and almost no effect at 16 μM Mn^{2+}. Consistent with these data, a similar minor decrease of the rate constant k_2 was observed in photoactivation experiments performed at lower (stoichiometric) concentrations of Mn^{2+} (1−4 μM) and 8 mM Ca^{2+} (*28*). As discussed below, the effect on λ_2 correlates with formation of Mn^{2+}−bicarbonate complexes in solution.

DISCUSSION

Optimal Mn^{2+}/Ca^{2+} Concentrations for Photoactivation. The present data extend the range of Mn^{2+}/Ca^{2+} concentrations which has been studied using the high-resolution kinetic measurements. Remarkably, over the entire range of Mn^{2+} and Ca^{2+} concentrations from 4 to 250 Mn^{2+}/PSII and 2−500 mM Ca^{2+} the time course of photoactivation quantitatively follows a two-step biexponential kinetic model of eq 1. To achieve a high photoactivation yield at high Mn^{2+} concentrations (100−250 μM), the Ca^{2+} concentration needs also to be increased to 0.1−0.5 M (Table 1), which is a 12−50-fold increase compared to 8 mM Ca^{2+} found optimal at the lower 8−16 μM Mn^{2+} concentrations (*23*). Intermediate Mn^{2+}/Ca^{2+} concentrations require about the same ratio. Thus, an approximately fixed ratio of Mn^{2+}:Ca^{2+} = 1:500 needs to be maintained in order to optimize the photoactivation yield. Ratios of 1:20 and 1:50 may be derived from the data presented in the works of others (*25*, *27*); the difference probably originates from the different illumination condition (continuous dim source light), different extrinsic protein content in the apo-WOC−PSII membranes, and different electron acceptors used in these studies.

The origin of this optimal Mn^{2+}/Ca^{2+} ratio can be explained by a simple model (Scheme 1) involving competitive binding of these cofactors at their (functional) effector sites (*20*, *24*, *27*). At Mn^{2+} concentrations below this optimal ratio, Ca^{2+} can bind to the Mn^{2+} binding site and thus shifts the initial equilibrium to an inactive dark precursor(s). The inactive species lack Mn^{2+} bound to the high-affinity site or have Ca^{2+} blocking Mn^{2+} at this site. Kinetic evidence for Ca^{2+} displacement of Mn^{2+} at the high-affinity site was previously presented in which the decay rate of IM_1 to IM_0 was shown to be proportional to the Ca^{2+} concentration (*23*). The active species in Scheme 1 have Mn^{2+} bound at the high-affinity site and thus can be photooxidized to form the next assembly intermediate. Inappropriate Ca^{2+} binding may delay or even block a photoassembly process with a partially assembled WOC−PSII, possibly leading to photoinhibition damage (*27*, *41*). Photoinhibition processes (reversible or irreversible) are known to occur to these inactive precursors owing to the absence of a photooxidizable electron donor and thus suppress the overall yield of the photoactivation process (*42*, *43*).

At Mn^{2+} concentrations at or higher than the optimal, the dark equilibrium is shifted to the active dark precursors (i.e., symbolized as [$Mn^{2+}(OH_2)$] in Scheme 1). This both increases the initial assembly rate and suppresses photoinhibition. However, as the Mn^{2+} concentration increases above the optimal Mn^{2+}/Ca^{2+} ratio, the photoactivation yield decreases due to competitive electron donation by excess (nonfunctional) Mn^{2+} ions. This delays the assembly process and exposes the partially assembled WOC−PSII to excessive photodamage. One of the physiological roles of Ca^{2+} was previously suggested to suppress the inappropriate ligation of Mn^{2+} to the partially assembled WOC and thereby promote the ligation of Mn^{2+} to productive sites which lead to assembly of the functional inorganic core (*41*). Thus, both excessively low and high Mn^{2+}/Ca^{2+} ratios result in partially assembled clusters and appreciable photoinhibition, while maintaining an optimal Mn^{2+}/Ca^{2+} ratio reduces this inhibition. With the Mn^{2+}/Ca^{2+} concentrations optimized, the photoactivation yield can increase to 60−70% at the higher cofactor concentrations, compared to only 20−30% at the lower cofactor concentrations (Table 1). This observation is consistent with Scheme 1, which predicts a shift from the inactive to active dark precursors when both Mn^{2+} and Ca^{2+} concentrations are proportionally increased. The increased concentrations also increase the availability of the Mn^{2+}/Ca^{2+} cofactors during all other steps of photoassembly.

Scheme 1: Proposed Intermediates in the First Steps of the Photoactivation Process at High Ca^{2+} Concentration[a]

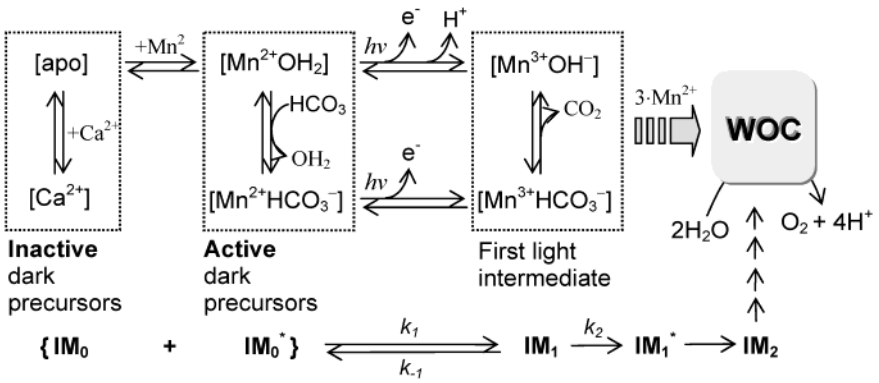

[a] Brackets represent the high-affinity Mn site on apo-WOC−PSII. Ca^{2+} is not shown but is assumed to be bound at its effector site on apo-WOC−PSII. Only one water ligand to Mn^{2+}/Mn^{3+} is shown which undergoes proton ionization; all other (protein-derived and water molecule) ligands are omitted for clarity.

These results suggest that biogenesis of the WOC cluster in vivo should be able to tolerate a wide range of environmental concentrations of Mn^{2+} and Ca^{2+} by controlling the intracellular *ratio* close to the optimal value of 1:500. This control may be important for proper assembly and functioning in vivo. WOC biogenesis and localization occur within different domains of the thylakoid membrane in chloroplasts (stromal vs granal membranes) (*44*), and in some cyanobacteria (*Gloeobacter v.*) it occurs within a single membrane system that is contiguous with the cytoplasmic membrane (*45*). Experimental data are rare on the intracellular concentrations of Mn^{2+} and Ca^{2+} within the lumenal space of the thylakoid membrane system of chloroplasts where the WOC cofactors are localized. However, an estimate of the mean number of Mn^{2+} ions within the unicellular cyanobacteria *Synechocystis* pcc6803 has been determined to be ca. 10^8/mature cell for cells grown under standard culture conditions (*46*). For an average cell diameter of 4 μm this corresponds to a mean concentration of about 3 mM. The majority of this Mn^{2+} is reversibly associated with the cytoplasmic membrane, while a smaller amount, typically 1−2%, is tightly associated with the internal thylakoid membrane. This estimate suggests that a 100-fold range in local Mn^{2+} concentrations is present internally within some unicellular cyanobacteria. Mn^{2+} stress can produce an additional 100-fold drop in the labile cytoplasmic Mn^{2+} stores (*46*). Thus, the present data indicate that a system for compartmentation of the WOC that suppress such large swings in internal metal ion concentration, or a system for cosequestration of Ca^{2+}, would seem to be needed for efficient assembly and function of the WOC in vivo.

Kinetic Rate Parameters and Mechanism. Over the broad range of cofactor concentrations (i.e., 10−250 μM Mn^{2+} and 8−500 mM Ca^{2+}) the kinetic parameters, λ_1 and λ_2, change by no more than a factor of 2, if their concentration ratio is maintained fixed at the optimal ratio (Table 1). At typical photoactivation conditions $\lambda_1 = k_1 + k_{-1}$, and thus λ_1 reflects both the forward and reverse processes in the formation of the first photooxidized intermediate (IM_1 in Scheme 1). The k_1 process involves several chemical steps, including site occupation by Mn^{2+} (both the free site and by displacement of Ca^{2+}), electron transfer to photooxidized tyrosine radical $Y_Z^{\bullet}$, and coupled proton transfer probably to a nearby amino acid base ($pK_a \sim 6-7$ (*30*, *47*)), resulting in formation of the first light intermediate [$Mn^{3+}(OH^-)$] (reviewed in refs *39* and *48*). The protonation state of other ligands to [Mn^{3+}], both protein-derived and water molecules, is not specified for simplicity. The light intermediate IM_1 decays through rereduction or dissociation processes with the decay rate k_{-1} or can also advance to the next light-induced assembly intermediate IM_2 through the rate-limiting step k_2 and IM_1* (Scheme 1).

Although in this work we did not attempt to determine the individual rate constants k_1 and k_{-1}, some conclusions can be drawn on the basis of earlier studies done at low Mn^{2+}/Ca^{2+} concentrations (*23*). The rate of formation of IM_1 (associated with rate constant k_1) was shown to increase with increasing Mn^{2+} concentration (at fixed Ca^{2+}) but decrease with increasing Ca^{2+} concentration (at fixed Mn^{2+}). Thus if both Mn^{2+} and Ca^{2+} concentrations are increased proportionally (i.e., to maintain their optimal ratio), the rate k_1 may not vary significantly. This observation is consistent with Scheme 1, which predicts that k_1 should depend on the concentration of the active precursor in the initial dark equilibrium. The decay rate k_{-1} was measured to be about an order of magnitude slower than k_1 and shown to increase linearly with the Ca^{2+} concentration (in the range 1−20 mM) while being nearly independent of Mn^{2+} concentration (*23*). This observation is also consistent with Scheme 1 where competition between Mn^{2+} and Ca^{2+} for binding to the high-affinity Mn^{2+} site is considered. Thus, λ_1 ($=k_1 + k_{-1}$) is a complex rate parameter, and its observed weak dependence over the wide range of Mn^{2+}/Ca^{2+} concentrations (Table 1) reflects off-setting processes, each having a different dependence on Mn^{2+} and Ca^{2+} concentrations.

The molecular process that occurs during the rate-limiting step λ_2 has not been identified yet. It was shown previously that λ_2 is a combination of dark and light steps. The first dark step may be associated with a slow protein conformational rearrangement that is triggered by the photooxidation of Mn^{2+} to Mn^{3+} (*39*). The slow rate of the λ_2 step [$\lambda_2 \sim (0.7-1.5) \times 10^{-3}$ s^{-1}] is compatible with, but not definitive evidence for, a protein-driven conformational change as the cause of overall slowness of this step (*24*). The weak dependence of λ_2 on Mn^{2+} and Ca^{2+} concentration (Table 1) is another indirect support of the kinetic limitation due to a slow protein conformational change. When the Mn^{2+} and Ca^{2+} concentrations are increased proportionally by 20-fold (i.e., keeping the Mn^{2+}/Ca^{2+} ratio fixed), the net result is apparent independence of λ_2 on the cofactor concentrations.

Previously, competition between Mn^{2+} and Ca^{2+} was found during the rate-limiting step λ_2 when their concentrations were independently varied both in large excess (*27*). At these conditions there is a population of other sites which create more intermediates, and thus a more complex kinetic behavior could be observed. Following the dark λ_2 step, a second photochemical step associated with the binding and oxidation of a second Mn^{2+} occurs and produces the long-lived intermediate IM_2 (*24*, *40*).

Bicarbonate Stimulation of Photoactivation. Our purpose now is using the model in Scheme 1 to identify the possible site(s) and mechanism of bicarbonate action in the photoassembly process. The present data demonstrate strong bicarbonate stimulation of the photoactivation yield Y_{SS} (Figures 5A) and the net rate of the first assembly step λ_1 (Figures 5B) at high cofactor concentrations. Both Y_{SS} and λ_1 exhibit the same concentration dependences on bicarbonate, which suggests a common origin of these effects. The amount of bicarbonate that produces the maximum effect on both of these parameters depends inversely on the Mn^{2+} concentration. By contrast, little or no effect is seen on the rate-limiting dark step λ_2 (Figure 5C).

To explain these effects, we propose that bicarbonate induces a shift in the initial dark equilibrium from an inactive to active Mn^{2+} precursor (Scheme 1) and that the most active species is a ternary complex bound to the high-affinity Mn^{2+} site in PSII, denoted $[Mn^{2+}(HCO_3^-)]$. This model predicts an inverse dependence on Mn^{2+} and bicarbonate concentrations. From the data in Figure 5 the formation constant for the ternary complex can be estimated to be 10^7 M^{-2} at pH 6, assuming a 1:1:1 apo-PSII:Mn^{2+}:HCO_3^- ternary complex in which only one HCO_3^- molecule participates in complex formation. Although the present data do not provide direct insight into the molecular nature of the Mn^{2+}−bicarbonate interaction, EPR results do show a bicarbonate effect on the ligand field parameters and the ^{55}Mn magnetic hyperfine interaction in the bound $[Mn^{3+}]$ (*49*). Taken together, the photoactivation and EPR data are consistent with each other and support the formation of a ternary complex. For the sake of simplicity we formulate the dark precursor as $[Mn^{2+}(HCO_3^-)]$, although the present data do not exclude ionization of a coordinated amino acid ligand to Mn^{2+}, e.g., $[Mn^{2+}(L^-)]$, or delivery of hydroxide to form $[Mn^{2+}(OH^-)]$. The bicarbonate effect is, however, not equivalent to alkalinization of the medium, which also accelerates λ_1 but greatly suppresses Y_{SS} (*30*).

Bicarbonate coordination to Mn^{2+} in solution results in a significantly lower oxidation potential to form Mn^{3+} than for aquo-Mn^{2+} (Mn^{2+}_{aq}) [$E° \sim 0.68-0.52$ vs 1.18 V, respectively (*50*, *51*)]. Similarly, a lower oxidation potential is expected for the bound $[Mn^{2+}(HCO_3^-)]$ compared to $[Mn^{2+}(OH_2)]$. Therefore, a higher quantum efficiency (and higher k_1 or lower k_{-1}) can be expected for the dark precursor $[Mn^{2+}(HCO_3^-)]$ during the first photochemical event of electron transfer to the oxidized $Y_Z^\bullet$. The oxidized $[Mn^{3+}(HCO_3^-)]$ may be more stable (lower k_{-1}) compared to $[Mn^{3+}(OH_2)]$ against decay by rereduction, which would improve the net efficiency of the first photochemical step. However, direct measurement of k_{-1} was not performed, so this possibility was not proven.

In contrast to λ_1, bicarbonate does not appreciably change the rate-limiting step (λ_2) at any concentration of Mn^{2+} and Ca^{2+} studied herein, in agreement with our earlier data at lower Mn^{2+} and Ca^{2+} concentrations (*28*). This observation is consistent with the proposal stated above that the λ_2 step is rate-limited by a dark conformation change in the protein and largely independent of the cofactor concentrations. At a high molar excess of Mn^{2+} over PSII, addition of millimolar concentrations of bicarbonate weakly decreases the photoactivation yield and slows both λ_1 and λ_2 rates (Figure 5). This effect coincides with the formation of free Mn^{2+}−bicarbonate complexes in solution and is in good agreement with the experimental dissociation constants for Mn^{2+}−bicarbonate complexes in water at pH 7: $Mn^{2+}(HCO_3^-)$ $K_D \sim 16$ mM (*52*) and $Mn^{2+}(HCO_3^-)_2$ $K_D \sim 30$ mM (*53*). As noted above, the electrochemical potentials of these complexes show they are much easier to oxidize than Mn^{2+}_{aq}, thus enabling them to serve as effective electron donors to PSII (*18*, *51*). We suggest that these species serve as competitive electron donors to oxidized $Y_Z^\bullet$, and possibly $Y_D^\bullet$ and $P680^+$ at nonfunctional sites that are not productive in photoassembly.

The present data on photoactivation kinetics corroborate the results reported earlier at low cofactor concentrations (1−8 μM Mn^{2+} and 8 mM Ca^{2+}), showing that bicarbonate weakly stimulates Y_{SS} and λ_1 but not λ_2 (*28*). The new results reported herein show that bicarbonate also acts at a second, lower affinity site populated at higher Mn^{2+} and Ca^{2+} concentrations. The high-affinity bicarbonate site is observable using stoichiometric Mn^{2+} concentration ($\leq$8 Mn/PSII) and causes maximal stimulations of Y_{SS} and λ_1 of 10−20% and saturates (disappears) above 8 Mn/PSII (*28*). The amount of bicarbonate needed to produce these changes is as little as 20 μM, which already saturates the effect seen at low Mn^{2+} and Ca^{2+} concentrations ($K_D < 10$ μM). Binding of bicarbonate to the low-affinity site is observable at 10-fold or greater Mn^{2+} and Ca^{2+} concentrations in the range 16−250 μM Mn^{2+} and causes a maximal increase of Y_{SS} by 70% and λ_1 by 300%. The amount of bicarbonate needed to half-saturate this site is 0.2−2 mM and depends reciprocally on the concentration of Mn^{2+}.

Thus, we can conclude that there are two sites or mechanisms for the bicarbonate effects on the photoactivation process, and these are visualized in Scheme 2. At low Mn^{2+}/Ca^{2+} concentrations (Scheme 2A) when the high-affinity Mn^{2+} site is unoccupied [$K_D = 30-40$ μM for Mn^{2+} has been recently estimated (*49*)], bicarbonate appears to electrostatically attract free Mn^{2+} to the vicinity of the PSII complex from solution. The increased concentration of Mn^{2+} would accelerate the rate of Mn^{2+} uptake during the photoactivation reaction and thus stimulate λ_1. Electrostatically induced rate stimulaton has been observed using lipophilic anions such as tetraphenylboron that partition into the PSII membrane (*30*). As depicted in Scheme 2, we propose that bicarbonate may serve as a membrane-soluble anion, as a base to ionize protein residues on the surface of the PSII protein complex, or form ion pairs with positively charged arginine residues on the surface of the D_1 protein in the PSII complex. The D_1 subunit of PSII contains three arginine residues located on the inner aqueous surface exposed to the lumen where the WOC assembly occurs. This stimulation effect is only observed if both bicarbonate and Mn^{2+} concentrations are kept below their saturation concentrations, e.g., below 20 μM bicarbonate or less than 8

Scheme 2: Two Proposed Sites/Mechanisms for Bicarbonate Stimulation of the Initial Step of the Photoactivation Reaction[a]

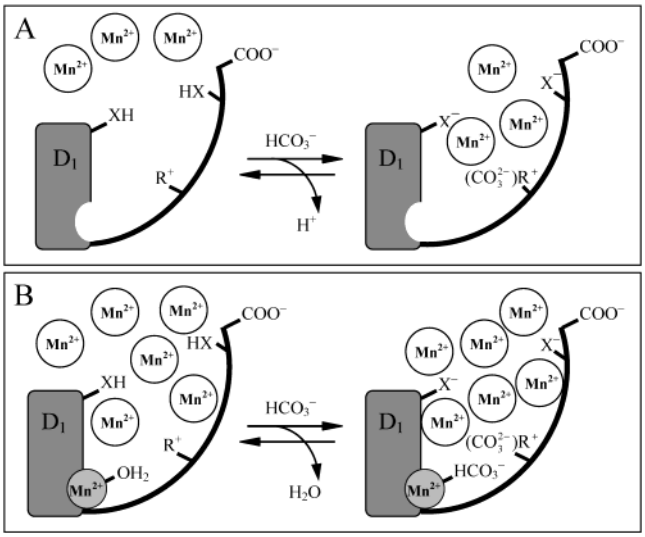

[a] (A) The high-affinity bicarbonate site. At low Mn^{2+} concentrations ($\leq$8 Mn^{2+}/PSII), bicarbonate anions electrostatically attract Mn^{2+} ions near the apo-WOC−PSI complex from solution by partitioning or ionization of protons or through ion pairing with cationic side chains (arginines, R^+) present in the D_1-carboxyl terminus (*28*). (B) The low-affinity bicarbonate site. At high Mn^{2+} concentrations ($\geq$30 Mn^{2+}/PSII), bicarbonate binds to the photoactive high-affinity Mn^{2+} binding site (*49*).

μM Mn^{2+}, and thus we call this the high-affinity site or mechanism of bicarbonate action (*28*).

The second site or mechanism of bicarbonate action is illustrated in Scheme 2B and occurs at higher cofactor concentrations (16−250 μM Mn^{2+} and 100−250 mM Ca^{2+}) and thus is dubbed the low-affinity site. The high-affinity Mn^{2+} site is occupied at these concentrations, and direct coordination of bicarbonate to this Mn^{2+} to form a ternary complex with apo-WOC−PSII, e.g., [$Mn^{2+}(HCO_3^-)$], is proposed as the origin of the low-affinity bicarbonate effect.

Bicarbonate Protects against Photoinhibition. The highest photoactivation yields we have found so far require bicarbonate (maximum Y_{SS} = 75% at 250 μM $MnCl_2$, 100 mM $CaCl_2$, and 125 μM bicarbonate, pH 6.0). The present and previous photoactivation data show that, at all concentrations of Mn^{2+} and Ca^{2+} that produce incomplete assembly of the inorganic core of the WOC, bicarbonate is able to significantly increase the rate and yield of productive intermediates and reduce the number of centers that become photoinactivated. This occurs at concentrations of bicarbonate that are physiologically important in cells and chloroplasts (*29*). Thus, bicarbonate should be considered an important native cofactor for photoassembly of the inorganic core of the WOC and photoprotection of the protein complex in oxygenic phototrophs.

ACKNOWLEDGMENT

We thank George Cheniae for stimulating discussions and encouragement through many years.

REFERENCES

1. van Rensen, J. J. S., Xu, C. H., and Govindjee (1999) Role of bicarbonate in photosystem II, the water-plastoquinone oxidoreductase of plant photosynthesis, *Physiol. Plant. 105*, 585−592.
2. Eaton-Rye, J. J., and Govindjee (1988) Electron-Transfer Through the Quinone Acceptor Complex of Photosystem-Ii After One or 2 Actinic Flashes in Bicarbonate-Depleted Spinach Thylakoid Membranes, *Biochim. Biophys. Acta 935*, 248−257.
3. Xu, C., Taoka, S., Crofts, A. R., and Govindjee (1991) Kinetic characteristics of formate/formic acid binding at the plastoquinone reductase site in spinach thylakoids, *Biochim. Biophys. Acta 1098*, 32−40.
4. Diner, B. A., and Petrouleas, V. (1990) Formation by NO of nitrosyl adducts (Part II), *Biochim. Biophys. Acta 1015*, 141−149.
5. Hienerwadel, R., and Barthomieu, C. (1995) Bicarbonate binding to the non-heme iron of Photosystem II investigated by Fourier transform infrared difference spectroscopy and 13C-labeled bicarbonate, *Biochemistry 34*, 16288−16297.
6. van Rensen, J. J. S., Tonk, W. J. M., and Debruijn, S. M. (1988) Involvement of Bicarbonate in the Protonation of the Secondary Quinone Electron-Acceptor of Photosystem-Ii Via the Non-Heme Iron of the Quinone-Iron Acceptor Complex, *FEBS Lett. 226*, 347−351.
7. Mende, D., and Wiessner, W. (1985) Bicarbonate Invivo Requirement of Photosystem-Ii in the Green-Alga Chlamydobotrys-Stellata, *J. Plant Physiol. 118*, 259−266.
8. Kamen, M. (1989) Onward into a fabulous half century, *Photosynth. Res. 21*, 137−144.
9. Stemler, A., and Govindjee (1973) Bicarbonate Ion as a Critical Factor in Photosynthetic Oxygen Evolution, *Plant Physiol. 52*, 119−123.
10. Metzner, H., Fischer, K., and Bazlen, O. (1981) in *Photosynthesis: Electron Transport and Photophosphorylation* (Akoynoglou, G., Ed.) pp 375−387, Balaban Publications, Philadelphia, PA.
11. Stemler, A. (1980) Inhibition of Photosystem II by formate. Possible evidence for a direct role of bicarbonate in photosynthetic oxygen evolution, *Biochim. Biophys. Acta 593*, 103−112.
12. Radmer, R., and Ollinger, O. (1980) Isotopic composition of photosynthetic O_2 flash yields in the presence of $H_2{}^{18}O$ and $HC^{18}O^-_3$, *FEBS Lett. 110*, 57−61.
13. Moubarakmilad, M., and Stemler, A. (1994) Oxidation−Reduction Potential Dependence of Photosystem-Ii Carbonic-Anhydrase in Maize Thylakoids, *Biochemistry 33*, 4432−4438.
14. Lu, Y. K., and Stemler, A. J. (2002) Extrinsic photosystem II carbonic anhydrase in maize mesophyll chloroplasts, *Plant Physiol. 128*, 643−649.
15. Klimov, V. V., and Baranov, S. V. (2001) Bicarbonate requirement for the water-oxidizing complex of photosystem II, *Biochim. Biophys. Acta 1503*, 187−196.
16. Klimov, V. V., Hulsebosch, R. J., Allakhverdiev, S. I., Wincencjusz, H., Van Gorkom, H. J., and Hoff, A. J. (1997) Bicarbonate May Be Required for Ligation of Manganese in the Oxygen-Evolving Complex of Photosystem Ii, *Biochemistry 36*, 16277−16281.
17. Campbell, K. A., Force, D. A., Nixon, P. J., Dole, F., Diner, B. A., and Britt, R. D. (2000) Dual-Mode EPR detects the initial intermediate in the photoassembly of the PSII Mn cluster, *J. Am. Chem. Soc. 122*, 3754−3761.
18. Kozlov, Y. N., and Klimov, V. V. (1998) Possible relationship of mechanisms of Mn2+-ions oxidation and the manganese cluster of the photosystem 2 plant formation, *Biol. Membr. 15*, 472−476.
19. Cheniae, G. M., and Martin, I. F. (1971) Photoactivation of Manganese Catalyst of O2 Evolution. 1. Biochemical and Kinetic Aspects, *Biochim. Biophys. Acta 253*, 167−181.
20. Ono, T.-A., and Inoue, Y. (1983) Requirement of divalent cations for photoactivation of the latent water-oxidation system in intact chloroplasts from flashed leaves, *Biochim. Biophys. Acta 723*, 191−201.
21. Burnap, R. L., Qian, M., and Pierce, C. (1996) The manganese-stabilizing protein of photosystem II modifies in vivo deactivation and photoactivation kinetics of the H_2O oxidation complex in *Synechocystis* sp. PCC6803, *Biochemistry 35*, 874−882.
22. Ananyev, G. M., and Dismukes, G. C. (1996) Assembly of the Tetra-Mn Site of Photosynthetic Water Oxidation by Photoactivation: Mn Stoichiometry and Detection of a New Intermediate, *Biochemistry 35*, 4102−4109.
23. Zaltsman, L., Ananyev, G., Bruntrager, E., and Dismukes, G. C. (1997) A quantitative kinetic model for photoassembly of the photosynthetic Water Oxidase from its inorganic constituents: requirements for Mn and Ca in the kinetically resolved steps, *Biochemistry 36*, 8914−8922.

24. Tamura, N., and Cheniae, G. M. (1987) Photoactivation of the water-oxidizing complex in Photosystem II membranes depleted of Mn and extrinsic proteins. I. Biochemical and kinetic characterization, *Biochim. Biophys. Acta 890*, 179−194.
25. Tamura, N., Inoue, Y., and Cheniae, G. M. (1989) Photoactivation of the Water-Oxidizing Complex in Photosystem- Ii Membranes Depleted of Mn, Ca and Extrinsic Proteins. 2. Studies on the Functions of Ca-2+, *Biochim. Biophys. Acta 976*, 173−181.
26. Ananyev, G. M., Shafiev, M. A., and Klimov, V. V. (1988) Pulse photoactivation of the oxygen evolution by particles of Photosystem II, deprived of water soluble proteins, *Biophysics (Russia) 33*, 637−643.
27. Miller, A.-F., and Brudvig, G. (1989) Manganese and calcium requirement for reconstruction of oxygen-evolution activity in manganese-depleted Photosystem II membranes, *Biochemistry 28*, 8181−8190.
28. Baranov, S. V., Ananyev, G. M., Klimov, V. V., and Dismukes, G. C. (2000) Bicarbonate Accelerates Assembly of the Inorganic Core of the Water-Oxidizing Complex in Manganese-Depleted Photosystem Ii: a Proposed Biogeochemical Role for Atmospheric Carbon Dioxide in Oxygenic Photosynthesis, *Biochemistry 39*, 6060−6065.
29. Price, G. D., Maeda, S., Omata, T., and Badger, M. R. (2002) Modes of active inorganic carbon uptake in the cyanobacterium, *Synechococcus* sp PCC7942, *Funct. Plant Biol. 29*, 131−149.
30. Ananyev, G. M., and Dismukes, G. C. (1996) High-Resolution Kinetic Studies of the Reassembly of the Tetra- Manganese Cluster of Photosynthetic Water Oxidation: Proton Equilibrium, Cations, and Electrostatics, *Biochemistry 35*, 14608−14617.
31. Berthold, D. A., Babcock, G. T., and Yocum, C. F. (1981) A highly resolved oxygen-evolving photosystem II preparation from spinach thylakoid membranes, *FEBS Lett. 27*, 231−234.
32. Ghanotakis, D. F., Babcock, G. T., and Yocum, C. F. (1984) Structural and catalytic prperties of the oxygen evolving complex: correlation of polypeptide and manganese release with the behavior of Z^+ in chloroplasts and a highly-resolved preparation of the PSII complex, *Biochim. Biophys. Acta 765*, 388−398.
33. Kashino, Y., Koike, H., and Satoh, K. (2001) An improved sodium dodecyl sulfate-polyacrylamide gel electrophoresis system for the analysis of membrane protein complexes, *Electrophoresis 22*, 1004−1007.
34. Ono, T., and Inoue, Y. (1984) Ca-2+-Dependent Restoration of O-2-Evolving Activity in Cacl2-Washed Ps-Ii Particles Depleted of 33-Kda; 24-Kda and 16-Kda Proteins, *FEBS Lett. 168*, 281−286.
35. Sandusky, P. O., DeRoo, C. L. S., Hicks, D. B., Yocum, C. F., Ghanotakis, D. F., and Babcock, G. T. (1983) in *The oxygen evolving system of plant photosynthesis* (Inoue, Y., Crofts, A. R., Govindgjee, Murata, N., Renger, G., and Satoh, K., Eds.) pp 189−199, Academic Press, Tokyo.
36. Hunziker, D., Abramowicz, D. A., Damoder, R., and Dismukes, G. C. (1987) Evidence for an Association Between a 33 Kda Extrinsic Membrane-Protein, Manganese and Photosynthetic Oxygen Evolution. 1. Correlation With the S2 Multiline Electron-Paramagnetic-Res Signal, *Biochim. Biophys. Acta 890*, 6−14.
37. Cole, J., Boska, M., Blough, N. V., and Sauer, K. (1986) Reversible and irreversible effects of alkaline pH on Photosystem II electron-transfer reactions, *Biochim. Biophys. Acta 848*, 41−47.
38. Ahlbrink, R., Haumann, M., Cherepanov, D., Bogershausen, O., Mulkidjanian, A., and Junge, W. (1998) Function of tyrosine Z in water oxidation by photosystem II: Electrostatical promotor instead of hydrogen abstractor, *Biochemistry 37*, 1131−1142.
39. Ono, T. (2001) Metallo-radical hypothesis for photoassembly of (Mn)(4)-cluster of photosynthetic oxygen evolving complex, *Biochim. Biophys. Acta 1503*, 40−51.
40. Ono, T. A., and Inoue, Y. (1987) Reductant-Sensitive Intermediates Involved in Multi-Quantum Process of Photoactivation of Latent O-2-Evolving System, *Plant Cell Physiol. 28*, 1293−1299.
41. Chen, C., Kazimir, J., and Cheniae, G. M. (1995) Calcium modulates the photoassembly of Photosystem II (Mn_4)-clusters by preventing ligation of nonfunctional high-valency states of manganese, *Biochemistry 34*, 13511−13526.
42. Blubaugh, D. J., and Cheniae, G. M. (1992) Photoassembly of the Ps2 Mn/Ca Cluster, *Photosynth. Res. 34*, 147.
43. Blubaugh, D. J., Atamian, M., Babcock, G. T., Golbeck, J. H., and Cheniae, G. M. (1991) Photoinhibition of Hydroxylamine-Extracted Photosystem-Ii Membranes—Identification of the Sites of Photodamage, *Biochemistry 30*, 7586−7597.
44. Mamedov, F., Stefansson, H., Albertsson, P. A., and Styring, S. (2000) Photosystem II in different parts of the thylakoid membrane: A functional comparison between different domains, *Biochemistry 39*, 10478−10486.
45. Mangels, D., Kruip, J., Berry, S., Rogner, M., Boekema, E. J., and Koenig, F. (2000) Photosystem I from the unusual cyanobacterium Gloeobacter violaceus, *Photosyn. Res. 72*, 307−319.
46. Keren, N., Kidd, M. J., Penner-Hahn, J. E., and Pakrasi, H. B. (2002) A Light-Dependent Mechanism for Massive Accumulation of Manganese in the Photosynthetic Bacterium *Synechocystis* sp. PCC 6803, *Biochemistry 41*, 15085−15092.
47. Ono, T. A., and Mino, H. (1999) Unique binding site for Mn2+ ion responsible for reducing an oxidized YZ tyrosine in manganese-depleted photosystem II membranes, *Biochemistry 38*, 8778−8785.
48. Ananyev, G. M., Zaltsman, L., Vasko, C., and Dismukes, G. C. (2001) The Inorganic Biochemistry of Photosynthetic Oxygen Evolution/Water Oxidation, *Biochim. Biophys. Acta 1503*, 52−68.
49. Baranov, S. V., Tyryshkin, A. M., Watt, R. K., and Dismukes, G. C., unpublished results.
50. Kozlov, Y. N., Kazakova, A. A., and Klimov, V. V. (1997) Changes in the redox-potential and catalase activity of Mn2+ ions during formation of Mn-bicarbonate complexes, *Biol. Membr. 14*, 93−97.
51. Dismukes, G. C., Klimov, V. V., Baranov, S. V., Kozlov, Y. N., Dasgupta, J., and Tyryshkin, A. M. (2001) The Origin of Atmospheric Oxygen on Earth: the Innovation of Oxygenic Photosynthesis, *Proc. Natl. Acad. Sci. U.S.A. 98*, 2170−2175.
52. Smith, R. M., and Martell, A. E. (1976) *Critical Stability Constants*, Vol. 4, Inorganic Complexes, Plenum, New York.
53. Kozlov, Y. N., and Klimov, V. V. (1997) Changes in the redox potential and catalase activity of Mn^{2+} ions during formation of Mn-Bicarbonate complexes, *Membr. Cell Biol. 11*, 115−120.

BI034858N